PHYSICAL REVIEW D **78,** 094502 (2008)

Magnetic moments of vector, axial, and tensor mesons in lattice QCD

Frank X. Lee and Scott Moerschbacher
Physics Department, The George Washington University, Washington, D.C. 20052, USA

Walter Wilcox
Department of Physics, Baylor University, Waco, Texas 76798, USA
(Received 2 August 2008; published 6 November 2008)

We present a calculation of magnetic moments for selected spin-1 mesons using the techniques of lattice QCD. This is carried out by introducing a progressively small static magnetic field on the lattice and measuring the linear response of a hadron's mass shift. The calculations are done on 24^4 quenched lattices using standard Wilson actions, with $\beta = 6.0$ and pion mass down to 500 MeV. The results are compared to those from the form factor method.

DOI: 10.1103/PhysRevD.78.094502 PACS numbers: 12.38.Gc, 13.40.Em, 14.40.−n

I. INTRODUCTION

Magnetic moment is a fundamental property of hadrons that arises from the linear response of a bound system to an external stimulus (in this case, magnetic field). It is a good testing ground for studying the internal structure of hadrons as governed by the quark-gluon dynamics of QCD, the fundamental theory of the strong interaction. Most efforts to compute the magnetic moment on the lattice come in two categories. One is the form factor method which involves three-point functions [1–7]. Another is the background field method using only two-point functions (mass shifts) [8–11]. The form factor method requires an extrapolation to zero momentum transfer $G_M(Q^2 = 0)$ due to the nonvanishing minimum discrete momentum on the lattice [12]. The background field method, on the other hand, can access the magnetic moment directly but is limited to static properties due to the use of a static field. Here we report a calculation of the vector meson magnetic moments in this method, parallel to a recent calculation in the form factor method [13]. We also report results on mesons in the axial and tensor sectors. Some of the preliminary results have been reported in a conference [14]. It is an extension of our earlier work on baryon magnetic moments [15] and electric [16] and magnetic polarizabilities [17] in the same method.

II. CORRELATION FUNCTIONS

The mass of a meson can be extracted from the time-ordered, two-point correlation function in the QCD vacuum, projected to zero momentum

$$G(t) = \sum_{\vec{x}} \langle \eta(x) \eta^\dagger(0) \rangle, \tag{1}$$

where η is the interpolating field of the meson under consideration. The general form of the interpolating field with a simple $\bar{q}_1 q_2$ quark content can be written as

$$\eta = \bar{q}_1 \Gamma q_2, \tag{2}$$

where Γ is a general gamma matrix that depends on the meson type. For the spin-1 mesons considered in this work, $\Gamma = \gamma_\mu$ for vector mesons, $\Gamma = \gamma_5 \gamma_\mu$ for axial mesons, and $\Gamma = \gamma_\mu \gamma_\nu$ for tensor mesons. Here we only consider mesons with different q_1 and q_2 to avoid the complication of disconnected loops.

On the quark level, Eq. (1) is evaluated by contracting out the quark pairs, yielding a function of quark propagators,

$$C(x, 0) = -\mathrm{Tr}[S_{q_1}(x, 0) \gamma_0 \Gamma^\dagger \gamma_0 \gamma_5 S^\dagger_{q_2}(x, 0) \gamma_5 \Gamma], \tag{3}$$

where the quark propagator $S_q(x, 0)$ is the inverse of the quark matrix $M = \gamma^\mu D_\mu + m_q$. The correlation function is defined as the Euclidean-space path integral over the gauge field G_μ,

$$G(t) = \sum_{\vec{x}} \frac{\int DG_\mu \det(M) e^{-S_G} C(x, 0)}{\int DG_\mu \det(M) e^{-S_G}}, \tag{4}$$

where S_G is the gauge action of QCD. On the lattice, the path integral is evaluated numerically by Monte Carlo methods. We use the quenched approximation in this work which corresponds to setting $\det(M)$ to a constant.

On the hadronic level, the correlation function is saturated by the complete spectrum of intermediate states

$$G(t) = \sum_i w_i e^{-m_i t}, \tag{5}$$

where m_i are the masses and w_i are spectral weights that are a measure of the ability of the interpolating field to excite or annhilate the states from the QCD vacuum. The ground state can be extracted by fitting $G(t)$ at large time.

To compute magnetic moments, we need to use polarized interpolating fields. For a magnetic field applied in the z direction, we use

$$\eta_\pm = \frac{1}{\sqrt{2}} \bar{q}_1 (\mp \Gamma_x - i \Gamma_y) q_2 = \frac{1}{\sqrt{2}} (\mp \eta_x - i \eta_y). \tag{6}$$

The interaction energies $E_\pm$ are extracted from the correlation functions

$$\langle \eta_\pm \eta^\dagger_\pm \rangle = \frac{1}{2} [\langle \eta_x \eta^\dagger_x \rangle \mp i (\langle \eta_x \eta^\dagger_y \rangle - \langle \eta_y \eta^\dagger_x \rangle) + \langle \eta_y \eta^\dagger_y \rangle]. \tag{7}$$

Equation (7) implies that the polarization comes from the imaginary parts of the off diagonal correlation between x and y components in the presence of the magnetic field. These imaginary parts are zero in the absence of the field, so they are responsible for the magnetic moments we observe. We use for vector mesons $\Gamma_x = \gamma_1$ and $\Gamma_y = \gamma_2$; for axial mesons $\Gamma_x = \gamma_5\gamma_1$ and $\Gamma_y = \gamma_5\gamma_2$; and for tensor mesons $\Gamma_x = \gamma_2\gamma_3$ and $\Gamma_y = \gamma_1\gamma_3$.

For each meson type, different quark combinations q_1 and q_2 correspond to different states. In the case of vector mesons, they are the well-known $\rho^+(\bar{d}u)$, $\rho^-(\bar{u}d)$, $\phi(\bar{s}s)$, $K^{*+}(\bar{s}u)$, $K^{*-}(\bar{u}s)$, and $K^{*0}(\bar{s}d)$. In the case of axial mesons, they are $a_1^+(\bar{d}u)$, $a_1^-(\bar{u}d)$, $K_1^{*+}(\bar{s}u)$, $K_1^{*-}(\bar{u}s)$, and $K_1^{*0}(\bar{s}d)$. In the case of tensor mesons, they are less well known and we call them $b_1^+(\bar{d}u)$, $b_1^-(\bar{u}d)$, $K_t^{*+}(\bar{s}u)$, $K_t^{*-}(\bar{u}s)$, and $K_t^{*0}(\bar{s}d)$. Counting the states with $\bar{s}s$ content (like the ϕ meson), we cover 18 states of spin-1 mesons.

III. BACKGROUND FIELD METHOD

For a particle of spin s in an uniform field with magnitude B,

$$E_\pm = m \pm \mu B, \tag{8}$$

where the upper sign means spin-up and the lower sign means spin-down relative to the magnetic field, and $\mu = g\frac{e}{2m}s$. We use the following method to extract the g factors:

$$g = m\frac{(E_+ - m) - (E_- - m)}{eBs}. \tag{9}$$

In order to place a magnetic field on the lattice, we construct an analogy to the continuum case. The covariant derivative of QCD is modified by the minimal coupling prescription

$$D_\mu = \partial_\mu + gG_\mu + qA_\mu, \tag{10}$$

where q is the charge of the fermion field and A_μ is the four-vector potential describing the background field. On the lattice, the gluon fields G_μ are introduced via link variables $U_\mu(x) = \exp(igaG_\mu)$. So the prescription amounts to multiplying a $U(1)$ phase factor $\exp(iqaA_\mu)$ to the gauge links. Choosing $A_y = Bx$ (which assumes a zero gauge potential at x = 0 relative to the source position), a constant magnetic field B can be introduced in the z direction. Then the phase factor is applied to the y-links

$$U_y \rightarrow \exp(iqaBx)U_y. \tag{11}$$

In our calculations, we use a linearized version for small field strengths [18]

$$U_y \rightarrow (1 + iqaBx)U_y. \tag{12}$$

The computational demand of such background field calculations can be divided into three categories. The first is a *fully dynamical* calculation. For each value of the field, a new dynamical ensemble is needed that couples to u quark ($q = 1/3$), d quark, and s quark ($q = -2/3$). This requires a Monte Carlo algorithm that can treat the three flavors distinctively. Quark propagators are then computed on the ensembles with matching field values. This has not been attempted. The second can be termed as the *reweighting* method in which a perturbative expansion of the action in terms of the field is performed. There has been an attempt [19] to compute the neutron electric polarizability in this method. It involves the evaluation of disconnected diagrams. The third is what we call $U(1)$ *quenched*. No field is applied in the Monte Carlo generation of the gauge fields, only in the valence quark propagation in the given gauge background. In this case, any gauge ensemble can be used to compute valence quark propagators.

We use standard Wilson actions on the 24^4 lattice at $\beta = 6.0$, both $SU(3)$ and $U(1)$ quenched, and six kappa values $\kappa = 0.1515, 0.1525, 0.1535, 0.1540, 0.1545, 0.1555$, corresponding to pion mass of about 1015, 908, 794, 732, 667, 522 MeV. The critical value of kappa is $\kappa_c = 0.1571$. The strange pion mass is set at $\kappa = 0.1535$. The source location for the quark propagators is (x,y,z,t)=(12,1,1,2). We analyzed 100 configurations. The following five dimensionless numbers $\eta = qBa^2 = +0.00036, -0.00072, +0.00144, -0.00288, +0.00576$ give four small B fields (two positive, two negative) at $eBa^2 = -0.00108, +0.00216, -0.00432, +0.00864$ for both u and d (or s) quarks. These field values do not obey the quantization condition for periodicity since the values given by the condition cause too strong (too large a mass shift) for the small-field-expansion method to work, and thus break gauge invariance required in the $U(1)$ field. To minimize the effects, we work with Dirichlet boundary conditions in the x direction and large N_x. In addition, we place the source in the middle of the lattice in the x direction so that quarks have little chance of propagating to the edge. We also use Dirichlet boundary conditions in the t direction to maximize the number of time slices for mass extraction. The same set of boundary conditions are applied in both the zero-field and with-field calculations. Although the results previously obtained under these conditions appear reasonable [15], the effects of the approximations [linearization in Eq. (12), nonquantized fields, zero of the gauge potential, Dirichlet boundary condition] should be examined quantitatively in future studies. One way to reduce finite-volume effects by patching the magnetic fields has been proposed in a recent study [20] of delta magnetic moments. To eliminate the contamination from the even-power terms, we calculate mass shifts both in the field B and its reverse $-B$ for each value of B, then take the difference and divide by 2. Another benefit of repeating the calculation with the field reversed is that by taking the average of $\delta m(B)$ and $\delta m(-B)$ in the same data set, one can eliminate the odd-powered terms in the mass shift. The coefficient of the leading quadratic term is directly related to the magnetic polarizability [17].

IV. RESULTS AND DISCUSSION

A. Vector mesons

Figure 1 displays a typical effective mass plot for ρ^+. Both the mass and the mass shifts are shown. Good plateaus exist for all six pion masses. The mass shifts are extracted from the time window 10 to 13, as indicated in the figure. Figure 2 shows the mass shifts, defined as $\delta m(B) = g(eBs)$ from Eq. (9), as a function of the field for the ρ^+ meson. The slope is proportional to the g factor. There is good linear behavior going through the origin at all the field values, an indication that contamination from the higher-power terms has been effectively eliminated by the $(\delta m(B) - \delta m(-B))/2$ procedure. This is also con-

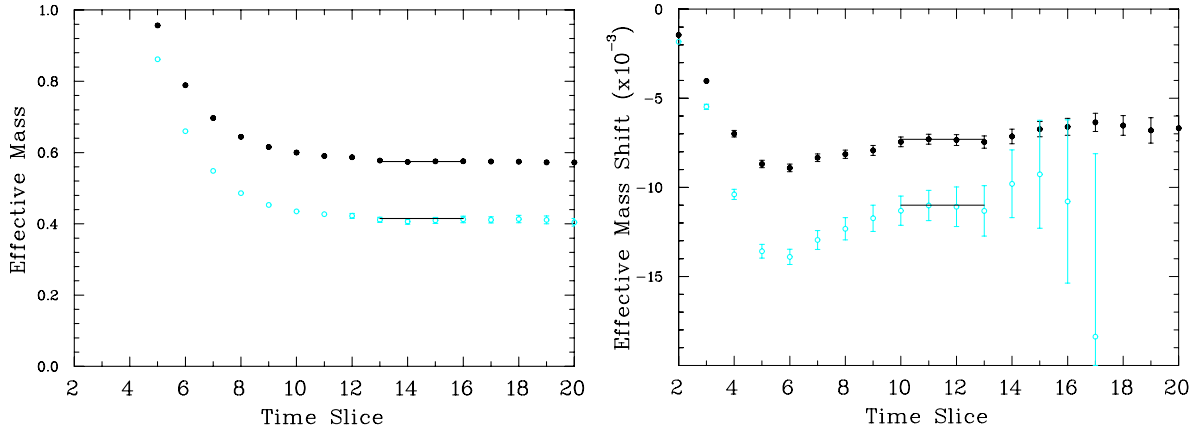

FIG. 1 (color online). Effective mass plot for the ρ^+ vector meson mass at zero field (left panel), and effective mass shifts at the weakest magnetic field (right panel) in lattice units. The solid and empty symbols correspond to the heaviest and lightest pion masses, respectively.

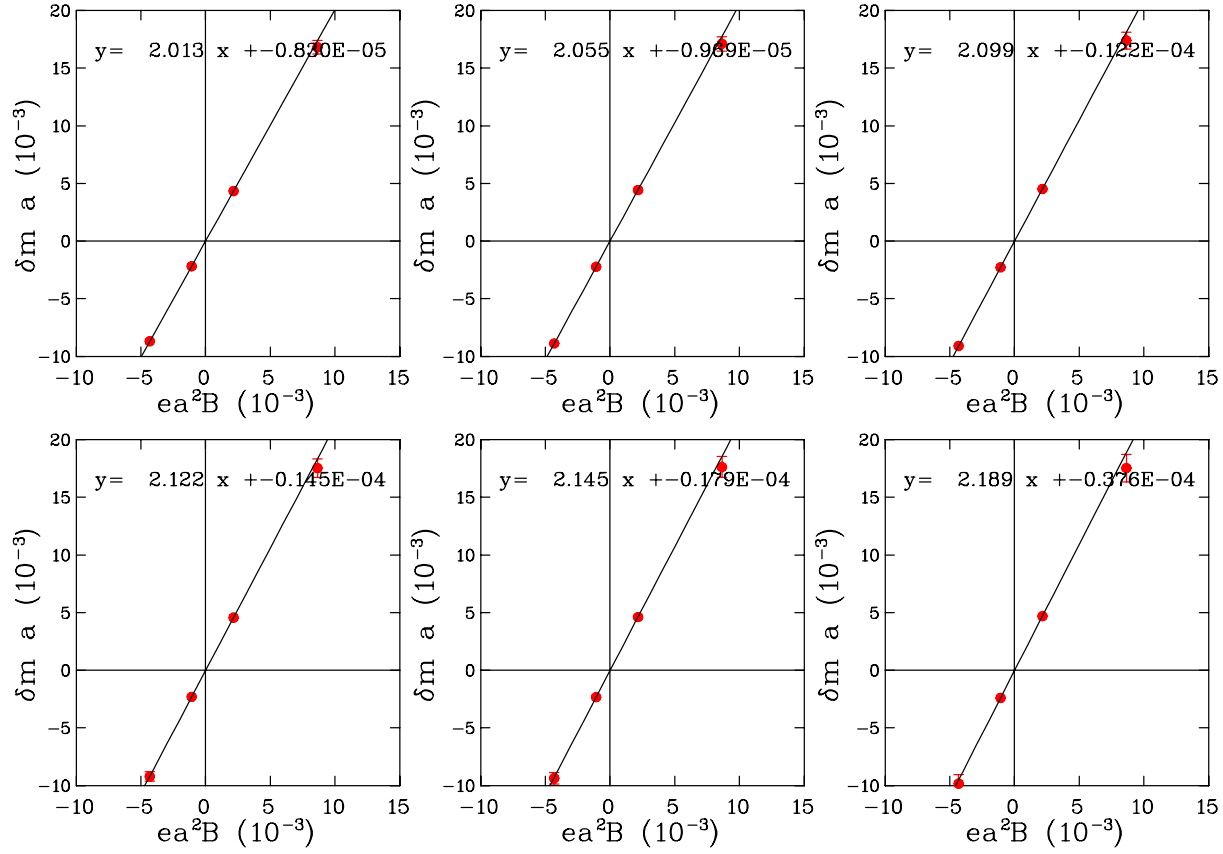

FIG. 2 (color online). Mass shifts for the ρ^+ meson as a function of the magnetic field in lattice units at the six pion masses (heavy to light from top left panel to right panel, then to bottom left panel to right panel). The slope of the mass shift at each pion mass gives the g factor corresponding to that pion mass. The line is a fit using only the two smallest B values.

firmed numerically by the smallness of intercept as shown in the fit results $y = ax + b$. At the lightest pion mass, there is a slight deviation from linear behavior at the stronger fields. For this reason, we only use the two smallest field values to do the linear fit at all the pion masses.

Figure 3 shows the g factors for the vector mesons as a function of pion mass squared. The lines are simple chiral fits using the ansatzs

$$g = a_0 + a_1 m_\pi, \tag{13}$$

and

$$g = a_0 + a_1 m_\pi + a_2 m_\pi^2. \tag{14}$$

They serve to show that there is onset of nonanalytic behavior as pion mass is lowered, so a linear extrapolation is probably desirable. But overall the g factors have a fairly weak pion-mass dependence. At large pion masses, the g factor of ρ^+ approaches 2, consistent with a previous lattice calculation using the charge-overlap method [21]. Our results for ρ^+ are slightly higher than those from the form factor method (see Fig. 8 in Ref. [13]). The results confirmed that $g_{\rho^-} = -g_{\rho^+}$ and $g_{K^{*-}} = -g_{K^{*+}}$ [22]. We also confirmed $g_{\rho^0} = 0$ numerically (not shown). These relations are expected from symmetries in the correlation functions: ρ^+ and ρ^- are charge conjugate pairs, and ρ^0 is charge conjugate eigenstate. The results also show that as far as g factors are concerned the ρ mesons are quite similar to their strange counterparts, the K^* mesons.

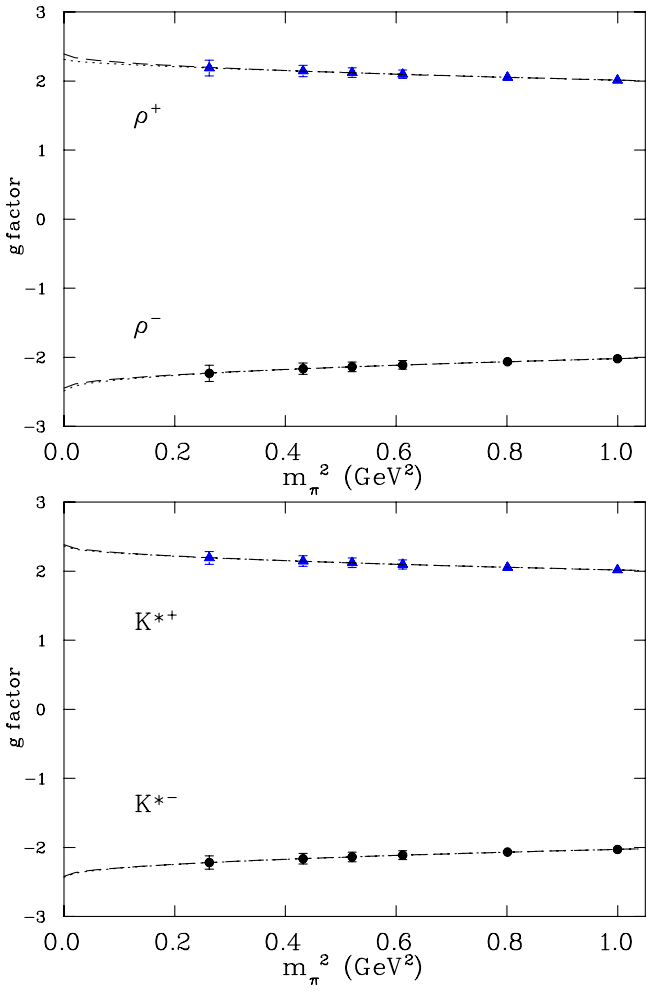

FIG. 3 (color online). g factors for the $\rho^\pm$ (top panel) and K^* (bottom panel) vector mesons as a function of pion mass squared. The 2 lines are chiral fits according to Eq. (13) (dashed line) and Eq. (14) (dotted line).

Note that the extracted g factors are in the particle's natural magnetons. To convert them into magnetic moments in terms of the commonly used nuclear magnetons (μ_N), we need to scale the results by the factor $938/M$ where M is the mass (in MeV/c^2) of the particle measured in the same calculation at each pion mass. Figure 4 shows a comparison of the results for ρ^+ and K^{*+}. The different pion-mass dependence between ρ^+ and K^{*+} mostly comes from that in the masses that are used to convert the g factors to magnetic moments. The values at the chiral limit extrapolated from Eq. (13) are $\mu_{\rho^+} = 3.25(3)\mu_N$ and $\mu_{K^{*+}} = 2.81(1)\mu_N$. There is no experimental information on these quantities. Compared to the form factor method (see Fig. 7 in [13]), our results are again a little higher. At the strange pion-mass point (the 3rd data point from the left), the two coincide to give a prediction for the magnetic moment of the $\phi(1020)$ meson, $\mu_\phi = 2.07(7)\mu_N$.

Figure 5 shows the results for K^{*0}. Our results confirm the expectation that $\mu_{K^{*0}}$ is small but has an interesting quark mass dependence. It is positive when the d quark is heavier than the s quark, exactly zero when they are equal, and turns negative when the d quark is lighter than the s quark. The same behavior has been observed in the form factor method (see Fig. 11 in [13]).

Figure 6 shows a direct comparison of the ρ^+ g factors from the background field method (this work) and the form

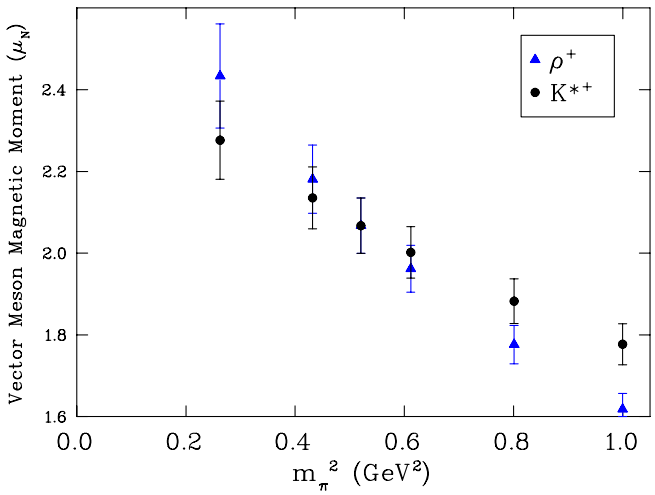

FIG. 4 (color online). Magnetic moments (in nuclear magnetons) for ρ^+ and K^{*+}.

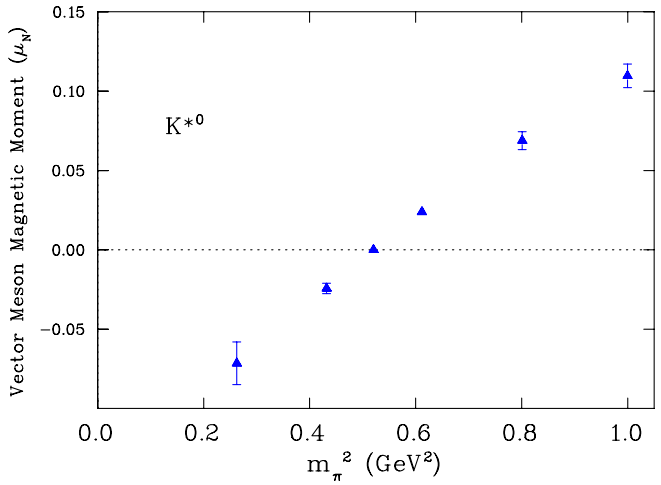

FIG. 5 (color online). Magnetic moment (in nuclear magnetons) for K^{*0}.

factor method [13]. The pion-mass coverage in the form factor results is deeper in the chiral regime (lowest about 300 MeV) than that in the background field results (lowest 500 MeV). The two results are consistent with each other within errors, which is remarkable considering the fact that they come from two completely different calculations. The errors displayed are statistical only, with 397 configurations in the form factor results and 100 configurations in the background field results.

B. Axial mesons

Figure 7 shows the effective mass shifts for the a_1^+ axial meson at the 2nd value of the magnetic field ($eBa^2 = 0.00216$). The signal is noisier compared to the vector case, but a plateau is still visible between time slice 3 to 5 in the mass shifts. Figure 8 shows the g factors for $a_1^\pm$ and

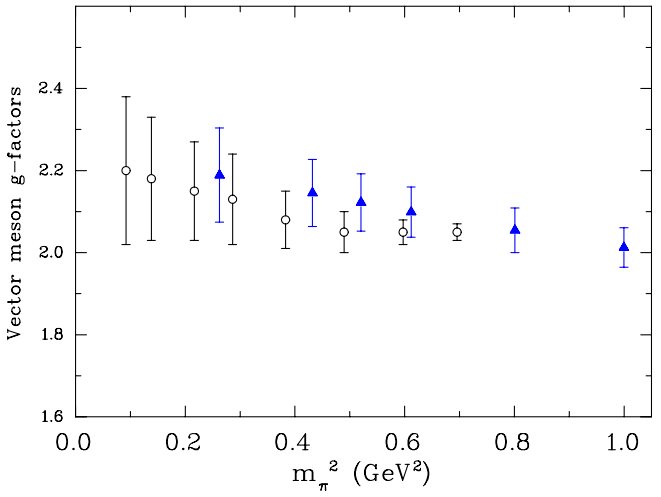

FIG. 6 (color online). Comparison of g factors for ρ^+ from this work (solid triangles) and the form factor method (empty circles) in Ref. [13].

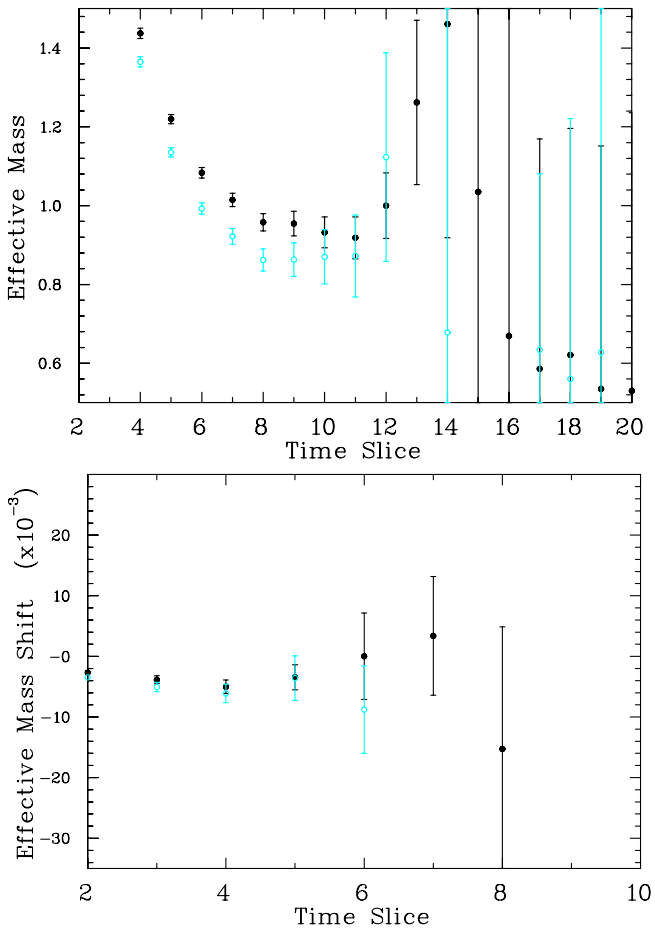

FIG. 7 (color online). Effective mass plot for the a_1^+ axial meson mass at zero field (top panel), and effective mass shifts at the 2nd weakest magnetic field (bottom panel) in lattice units. The solid and empty symbols correspond to the heaviest and 2nd lightest pion masses, respectively.

$K_1^{*\pm}$ extracted from this window at the six pion masses. The g factors are very similar to their counterparts in the vector channel (see Fig. 3). Figure 9 shows the g factors for K_1^{*0}. They are small as expected, but have a linear behavior across the zero as a function of the pion mass squared. Interestingly, they have the opposite sign to that in the vector channel (see Fig. 5): negative when the d quark is heavier than the s quark, exactly zero when they are equal, and turns positive when the d quark is lighter than the s quark.

C. Tensor mesons

Figure 10 shows the effective mass shifts for the b_1^+ tensor meson at the 2nd value of the magnetic field. The signal is much noisier than the axial case. It takes a long time (after step 10) for the zero-field mass to plateau and there is no convincing plateau in the mass shifts. The results are a demonstration of the difficulty of extracting a signal in this channel. Obtaining a reliable signal remains a challenge for future work.

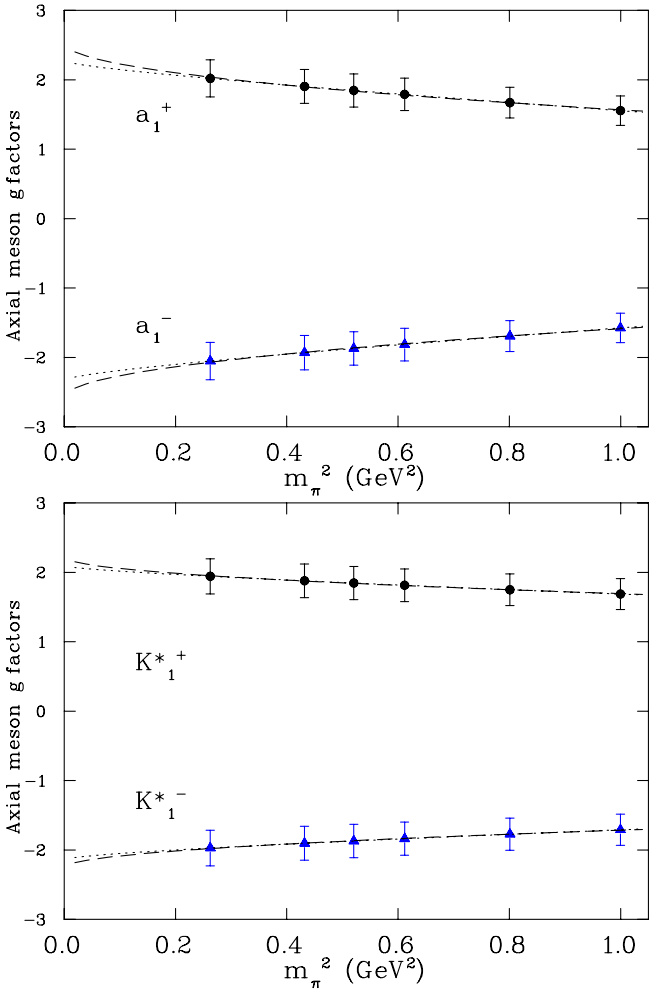

FIG. 8 (color online). g factors for the $a_1^{\pm}$ (top panel) and $K_1^{*\pm}$ (bottom panel) axial mesons as a function of pion mass squared. The 2 lines are chiral fits according to Eq. (13) (dashed line) and Eq. (14) (dotted line).

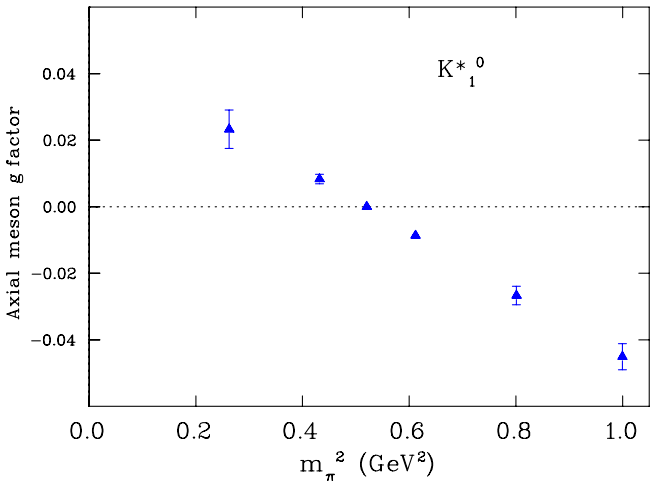

FIG. 9 (color online). g-factor for the neutral axial meson K_1^{*0}.

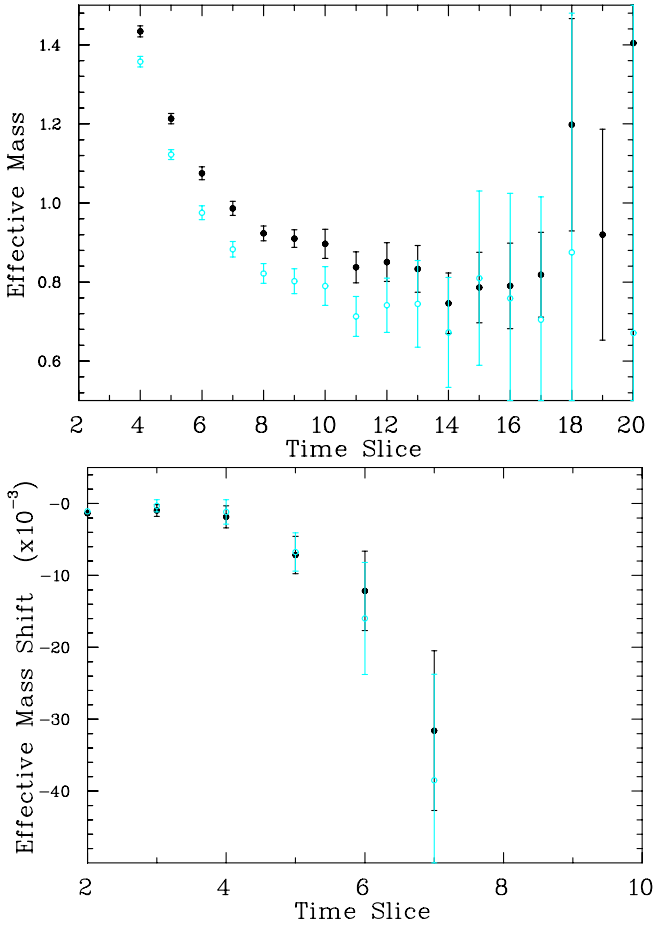

FIG. 10 (color online). Effective mass plot for the b_1^+ tensor meson mass at zero field (top panel), and effective mass shifts at the 2nd weakest magnetic field (bottom panel) in lattice units. The solid and empty symbols correspond to the heaviest and 2nd lightest pion masses, respectively.

V. CONCLUSION

In conclusion, we have computed the magnetic moment of vector, axial, and tensor mesons on the lattice using the background field method and standard lattice technology. The numerical results are summarized in Table I. Our results for the vector mesons are consistent with those from the form factor method, where a comparison is possible. The results for the axial and mesons are new. There is no convincing signal for the tensor mesons. Nonetheless, our results demonstrate that the method is robust and relatively inexpensive. Only mass shifts are required. There is no experimental information on these quantities so the lattice results can serve as a guide from first principles. Since the feasibility of the method is extended to the meson sector, the calculation can be improved in a number of ways. First, some of the approximations used in this calculation should be quantitatively examined, such as linearization, zero of the gauge potential, nonquantized fields, and Dirichlet boundary conditions, preferably on

TABLE I. The computed g factors for the spin-1 mesons as a function pion mass. The last column is a simple chiral extrapolation according to Eq. (13).

κ	0.1515	0.1525	0.1535	0.1540	0.1545	0.1555	Extrap.
m_π (GeV)	1.000	0.895	0.782	0.721	0.657	0.512	
Vector mesons							
$\rho^\pm$	2.01(4)	2.05(5)	2.10(6)	2.12(7)	2.14(8)	2.19(11)	2.39(1)
$K^{*\pm}$	2.02(5)	2.06(6)	2.10(7)	2.12(7)	2.15(8)	2.19(9)	2.38(1)
K^{*0}	0.125(8)	0.075(6)	0.025(3)	0.000	−0.024(3)	−0.089(13)	
Axial mesons							
$a_1^\pm$	−1.57(21)	−1.69(22)	−1.81(23)	−1.87(24)	−1.93(25)	−2.05(26)	−2.58(3)
$K_1^{*\pm}$	−1.71(22)	−1.77(23)	−1.84(24)	−1.87(24)	−1.90(24)	−1.97(26)	−2.26(1)
K_1^{*0}	−0.045(4)	−0.027(3)	−0.009(1)	0.000	0.008(1)	0.023(6)	

different volumes. One example is to patch the magnetic fields as proposed in Ref. [20] to reduce finite-volume effects. Second, more statistics are needed in the axial and tensor cases to better isolate the signals. Third, there is a need to push the calculations to smaller pion masses so that reliable chiral extrapolations can be applied. Fourth, the calculation should be extended to full QCD in order to see the effects of the quenched approximation, both in the $SU(3)$ sector and in the $U(1)$ sector. With the availability of dynamical configurations, all of the improvements can be made at the same time. In particular, the $U(1)$ effect in the sea quarks can be evaluated by reweighting the determinants in the correlation functions, without the need to generate new dynamical ensembles.

ACKNOWLEDGMENTS

This work is supported in part by the U.S. Department of Energy under Grant No. DE-FG02-95ER40907. W. W. acknowledges a research leave from Baylor University. The computing resources at NERSC and JLab have been used.

[1] G. Martinelli and C. T. Sachrajda, Nucl. Phys. **B316**, 355 (1989).
[2] D. B. Leinweber, T. Draper, and R. M. Woloshyn, Phys. Rev. D **43**, 1659 (1991); **46**, 3067 (1992); **48**, 2230 (1993).
[3] W. Wilcox, T. Draper, and K. F. Liu, Phys. Rev. D **46**, 1109 (1992).
[4] V. Gadiyak, X. Ji, and C. Jung, Phys. Rev. D **65**, 094510 (2002).
[5] M. Göckeler *et al.*, Phys. Rev. D **71**, 034508 (2005).
[6] J. Zanotti, Boinepalli, D. B. Leinweber, A. W. Williams, and J. B. Zhang, Nucl. Phys. B, Proc. Suppl. **128**, 233 (2004).
[7] I. C. Cloet, D. B. Leinweber, and A. W. Thomas, Phys. Lett. B **563**, 157 (2003).
[8] G. Martinelli *et al.*, Phys. Lett. **116B**, 434 (1982).
[9] C. Bernard, T. Draper, and K. Olynyk, Phys. Rev. Lett. **49**, 1076 (1982); C. Bernard, T. Draper, K. Olynyk, and M. Rushton, Nucl. Phys. **B220**, 508 (1983).
[10] J. Smit and J. C. Vink, Nucl. Phys. **B286**, 485 (1987).
[11] H. R. Rubinstein, S. Solomon, and T. Wittlich, Nucl. Phys. **B457**, 577 (1995).
[12] W. Wilcox, Phys. Rev. D **66**, 017502 (2002).
[13] J. N. Hedditch, W. Kamleh, B. G. Lasscock, D. B. Leinweber, A. G. Williams, and J. M. Zanotti, Phys. Rev. D **75**, 094504 (2007).
[14] F. X. Lee, S. Moerschbacher, and W. Wilcox, Proc. Sci., LATTICE2007 (2007) 151.
[15] F. X. Lee, R. Kelly, L. Zhou, and W. Wilcox, Phys. Lett. B **627**, 71 (2005).
[16] J. Christensen, W. Wilcox, F. X. Lee, and L. Zhou, Phys. Rev. D **72**, 034503 (2005).
[17] F. X. Lee, L. Zhou, W. Wilcox, and J. Christensen, Phys. Rev. D **73**, 034503 (2006).
[18] H. R. Fiebig, W. Wilcox, and R. M. Woloshyn, Nucl. Phys. **B324**, 47 (1989).
[19] M. Engelhardt, Phys. Rev. D **76**, 114502 (2007).
[20] C. Aubin, K. Orginos, V. Pascalutsa, and M. Vanderhaeghen, arXiv:0809.1629.
[21] W. Anderson and W. Wilcox, Ann. Phys. (N.Y.) **255**, 34 (1997).
[22] The g factors of both positively charged and negatively charged mesons should be the same. Here we calculate the g factor of negatively charged particles and compare it to positive ones as a test of the lattice data.